Journal of Inorganic and Organometallic Polymers and Materials
https://doi.org/10.1007/s10904-023-02921-4

RESEARCH

A Bis(terpyridine)nickel(II)-Based Coordination Nanosheet: A Redox-Active Material with Flexibility and Transparency

Kenji Takada[1] · **Hiroaki Maeda**[1] · **Hiroshi Nishihara**[1]

Received: 29 September 2023 / Accepted: 27 October 2023

Abstract
We report a novel functional bis(terpyridine)metal(II) complex coordination nanosheet (CONASH) comprising a three-armed terpyridine ligand and Ni^{2+} ion. The colourless Ni-terpyridine CONASH was synthesized by the method of interfacial coordination reaction at an interface of two immiscible liquids. The synthesized CONASH was characterized with various microscopic observations such as TEM, SEM, and AFM, and spectroscopic measurements such as XPS, IR, SEM/EDS, and UV–Vis spectroscopy. The bis(terpyridine)nickel(II) complex nanosheet demonstrated redox-activity stemming from terpyridine complexes without distinctive colour change. Thus, the bis(terpyridine)nickel(II) coordination nanosheet is a potential redox-active material with colourlessness and flexibility, necessary for future transparent electronics.

Keywords Coordination nanosheets · Terpyridine complexes · Electrochemistry

1 Introduction

Since the discovery of graphene [1], extensive studies have revealed various types of novel two-dimensional polymers such as transition metal dichalcogenides [2, 3], covalent organic frameworks [4, 5], and carbon allotropes [6–8]. Coordination nanosheets (CONASHs) are bottom-up-type, two-dimensional polymers woven through coordination reactions of molecular, ionic, or atomic components [9–13]. Due to the diversity of their chemical and physical properties arising from an infinite variety of ligand and metal ions, CONASHs have attracted considerable attention. Functional CONASHs tethering 1,2-dithiolate and its analogues [14–23], carboxylate [24, 25], dipyrromethine [26, 27], and polypyridyl [28–37] ligands have been developed.

Among coordination nanosheets, the family of tpy-based CONASHs (tpy: 2,2′:6′,2″-terpyridine) has been widely studied because tpy enables coordination to various metal ions such as Fe^{2+}, Co^{2+}, Zn^{2+}, and Pb^{2+} [28–37]. While Fe and Co-based terpyridine complexes are especially interesting due to their distinct redox-activities, $Ni(tpy)_2$-type coordination polymers are less arrestive than their Fe or Co counterparts, in spite of attractive redox-activity and catalytic activity of $[Ni(tpy)_2]^{2+}$ motifs [38, 39]. Here we introduce a redox-active terpyridine-based CONASH **1-Ni** comprising a three-fold symmetric terpyridine ligand **1** (1,3,5-tris(4-(4′-2,2′:6′,2″-terpyridyl)phenyl)benzene) and Ni^{2+} ions (Fig. 1). While some $Ni(tpy)_2$-based CONASHs have recently been explored for their catalytic activity in CO_2 reduction reactions [40], electrochemistry of $Ni(tpy)_2$-based CONASHs itself has not been unveiled yet. According to our knowledge, this is the first report of bis(terpyridine)nickel(II) complex-based coordination polymers focusing on their appearance on redox activity. A colourless multilayered nanosheet film was obtained via a simple liquid–liquid interfacial coordination reaction, and characterized by various microscopic and spectroscopic techniques. We focused smooth redox behaviour of **1-Ni** upon the oxidation of $[Ni(tpy)_2]^{2+}$ centres with charge storage of 3.6 C cm^{-3}, maintaining its colourlessness. Thus, **1-Ni** is a promising redox-active, flexible, and colourless material, which is necessary for future transparent electronics [41–43].

✉ Kenji Takada
takada.k.ag@rs.tus.ac.jp

✉ Hiroshi Nishihara
nisihara@rs.tus.ac.jp

Hiroaki Maeda
h-maeda@rs.tus.ac.jp

[1] Research Institute for Science and Technology, Tokyo University of Science, 2641, Yamazaki, Noda, Chiba 278-8510, Japan

Published online: 27 November 2023

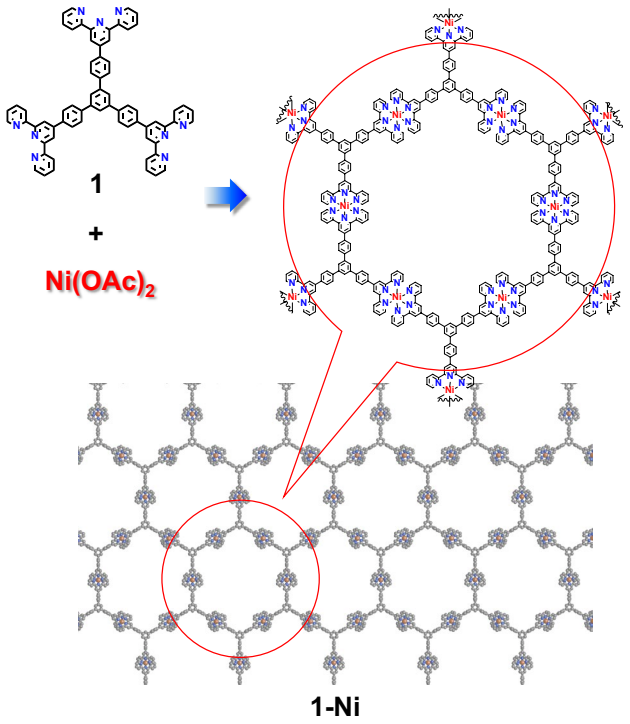

Fig. 1 Molecular structure of terpyridine ligand **1** and image of bis(terpyridine)nickel(II) CONASH, **1-Ni**

2 Experimental

2.1 Materials

Ligand **1** was prepared according to the method written in the literature [44]. $Ni(OAc)_2{\cdot}4H_2O$, $NiCl_2$, and 2,2′:6′,2″-terpyridine were purchased from Kanto Chemical Co. Ltd. or Tokyo Chemical Inc., and used without further purification. CH_2Cl_2 and CH_3CN were purchased from Kanto Chemical Co., Inc., and purified with Glass Contour Solvent Dispersing System (Nikko Hansen & Co., Ltd.). Acetone, methanol, and ethanol were purchased from Kanto Chemical Co., Inc., and used as received. Water was purified with Milli-Q purification system (Merck KGaA). Bu_4NPF_6 and Bu_4NClO_4 were purchased from Tokyo Chemical Inc., and recrystallized from hot ethanol, then dried in vacuo.

2.2 Preparation of Substrates

Indium tin oxide-coated glass substrate (ITO/glass substrates) were commercially available and washed under ultrasonication with following solvents successively: Acetone (HPLC grade, 5 min × 2), pure water (5 min × 2), detergent solution, pure water (5 min × 3), then ethanol (HPLC grade, 10 min × 3). Si (111) wafer (P type, B doped, ≤ 0.005 Ω cm, E&M Corporation) and Si(100) wafer (No-doped, E&M Corporation) were cut into small pieces, and used as a Si substrate. Quartz substrates were purchased from Monotech Inc., Ltd., and washed with fuming nitric acid before use. F-doped SnO_2-coated glass substrates (FTO/glass, ALLIANCE Biosystems, Inc.) were washed under ultrasonication with dichloromethane, ethanol and water successively.

2.3 Characterization

TEM measurements were carried out with Hitachi HF2000 equipped with an AMT-CCD camera with an acceleration voltage of 75 kV. A suspension of the nanosheet flakes in CH_2Cl_2 and ethanol was dropped onto a copper grid or an elastic carbon grid, and dried under vacuum overnight. FE-SEM images were recorded using JEOL JSM-7400FNT equipped with an EDS analyser. The acceleration voltage was set to 15 and 4 kV for SEM observation and SEM/EDS mapping, respectively. Samples for the FE-SEM observation was prepared by depositing **1-Ni** on a Si substrate. XPS was measured using PHI 5000 Versa Probe (ULVAC-PHI). Al Kα (15 kV, 25 W or 20 kV, 100 W) radiation was used as an X-ray source. The sample was deposited on a piece of a conductive carbon tape. The spectra were analysed using a MultiPak Software, and the binding energy was standardized using a C 1 s peak at 284.6 eV. In order to quantify the element abundance of the nanosheet, $[Ni(tpy)_2](BF_4)_2{\cdot}CH_3OH$ was employed as a standard compound which gives atomic ratio of N: Ni = 6: 1. Attenuated total reflection (ATR)-IR spectrum was recorded using a Thermo Scientific FT-IR Nicolet iS50 spectrometer. **1-Ni** deposited on a Si substrate was used and the spectrum of Si substrate was subtracted as a background. UV–vis spectra were obtained with a JASCO V570 spectrometer. AFM images were collected using an Agilent Technologies 5500 Scanning Probe Microscope. AFM was carried out using a silicon cantilever PPP-NCL or NCH (Nano World) in the high amplitude mode (Tapping Mode) under an ambient condition. The sample was prepared in the same way as that for the FE-SEM measurement.

2.4 Electrochemical Measurement

A series of electrochemical measurements was conducted using ALS 650B, ALS 650DT, and ALS 750E electrochemical analysers. For the analysis of Ligand **1** and $[Ni(tpy)_2](BF_4)_2{\cdot}CH_3OH$, a homemade glassy carbon working electrode, a Pt wire counter electrode, and an Ag^+/Ag reference electrode (0.01 M $AgClO_4$ in 0.1 M Bu_4NClO_4/CH_3CN) were used. As a supporting electrolyte solution, 0.1 M Bu_4NPF_6 solution of CH_3CN and 0.1 M Bu_4NClO_4 solution of CH_2Cl_2 were used. For the analysis of **1-Ni**, CH_2Cl_2 was

dried over activated molecular sieves 4A. An ITO or FTO substrate modified with **1-Ni**, dried under vacuum at 120 °C overnight, was used as a working electrode (0.478 or 0.264 cm^2), while a Pt wire was used as a counter electrode. A homemade Ag^+/Ag reference electrode (0.01 M $AgClO_4$ in 0.1 M Bu_4NClO_4/CH_3CN) was employed. As a supporting electrolyte solution, 1 M Bu_4NClO_4 or Bu_4NPF_6 solution in CH_2Cl_2 was used. The potential was standardized using the redox potential of ferrocenium/ferrocene redox couple measured using the reference electrode mentioned above. Spectroelectrochemical measurement was performed using a homemade electrochemical cell described in the literature [45]. All electrochemical measurements were carried out at room temperature.

2.5 Preparation of 1-Ni

A 0.1 mM solution of **1** in CH_2Cl_2 was prepared by dissolving 1 mg of **1** into 10 mL of CH_2Cl_2, and the solution was filtrated prior to use. The solution was poured into a vial with a diameter of 40 mm, then pure water (10 mL) was allowed to cover the solution of **1** to form a water/oil interface. An aqueous solution of $Ni(OAc)_2$ (50 mM, 10 mL, filtrated before use) was then added to the water phase by slow pipetting. After waiting for 3 days, **1-Ni** emerged at the interface as a pale orange film. The aqueous layer was replaced with pure water, followed by removal of both organic and aqueous phases. Ethanol and CH_2Cl_2 were added to **1-Ni** resulting in a CH_2Cl_2-ethanol mixture containing **1-Ni** flakes. **1-Ni** was then collected by filtration, and dried in vacuo.

2.6 Preparation of $[Ni(tpy)_2](BF_4)_2 \cdot CH_3OH$

In methanol (50 mL), 2,2′:6′,2″-terpyridine (93.5 mg, 401 µmol) and anhydrous nickel chloride (26.7 mg, 206 µmol) were refluxed for 1 h. After cooling the mixture to room temperature, excess ammonium tetrafluoroborate (1.017 g) was added. Resulting precipitate was collected by filtration and washed with methanol and diethyl ether, followed by drying under vacuum. Yield: 82.8 mg, 56.5%. Elemental analysis: found, C 51.06, H 3.45, N 11.94; calcd for $C_{30}H_{22}N_6NiB_2F_8 \cdot CH_3OH$, C 50.94, H 3.59, N 11.50.

2.7 Transfer of 1-Ni on Substrates

In order to transfer a small piece of the nanosheet onto a flat substrate, nanosheet flakes were re-dispersed in a mixture of CH_2Cl_2 and ethanol. The suspension was dropped onto a substrate using a pipette. After the solvent was evaporated, the modified substrate was dried with an Ar blow. **1-Ni** for spectroscopy and electrochemical measurements was deposited onto an ITO substrate by following methods; Substrates were immersed into an organic phase before performing the liquid/liquid interfacial coordination reaction. After the synthesis of **1-Ni**, both organic and aqueous phases were removed to allow the nanosheet to cover the substrate. The modified substrate was rinsed with H_2O, ethanol, and CH_2Cl_2 successively and dried under Ar blow.

3 Results and Discussion

3.1 Synthesis and Characterization

1-Ni was prepared using a liquid–liquid interfacial coordination reaction that was developed for fabrication of multilayered CONASH films with high aspect ratios of centimetre-scale 2D size and sub-micrometre-scale thickness [13]. For **1-Ni**, an aqueous solution of nickel acetate tetrahydrate (25 mM) was layered on a dichloromethane solution of ligand **1** (0.1 mM) in a glass vial with 40 mm in diameter. Keeping the interface calm for 3 days promoted gradual growth of **1-Ni** covering the entire interface (Fig. 2a). The reaction was quenched by dilution of the aqueous phase by repeated removal of the aqueous solution and addition of pure water to the aqueous phase. After the concentration of Ni^{2+} in the aqueous phase decreased to less than 0.1 mM, removal of all solvents and successive addition of pure ethanol gave flakes of **1-Ni** floating in ethanol (Fig. S1a). Floating **1-Ni** is almost invisible and highly flexible. **1-Ni** can be transferred easily onto various substrates such as Si, quartz, ITO/glass, FTO/glass and flexible plastic substrates. **1-Ni** on an ITO/glass substrate looks almost colourless, so that we can clearly read the letters "$Ni(tpy)_2$" printed on the paper located under **1-Ni**-decorated ITO substrate (Fig. 2b). **1-Ni** on a plastic is highly flexible (Fig. S1b), revealing good flexibility of the nanosheet.

The morphology of **1-Ni** was characterized by microscopy techniques. As with previously reported tpy-based CONASHs [32–34], **1-Ni** afforded neither X-ray nor electron diffraction patterns, plausibly because of low crystallinity stemming from randomly located counter-anions (CH_3COO^-), and disorder or mismatches in both in-plane and out-of-plane layer formation. We also tried the synthesis of **1-Ni** from other Ni salts such as $Ni(BF_4)_2$, $NiSO_4$, and nickel(II) *p*-toluenesulfonate. However, none of them gave diffraction pattern enough to resolve their precise molecular structures. Thus, instead, electron and atomic force microscopes were helpful to determine the morphology. The folded edge structure of **1-Ni** in the transmission electron microscope (TEM) image (Fig. 2c) suggested the layered nanosheet-like morphology of **1-Ni**. Additionally, the scanning electron microscope (SEM) image of **1-Ni** on a Si substrate reveals the flat surface of the nanosheet (Fig. 2d). Energy dispersive X-ray spectroscopy mapping under SEM observation (SEM/EDS) confirms that the observed flat film

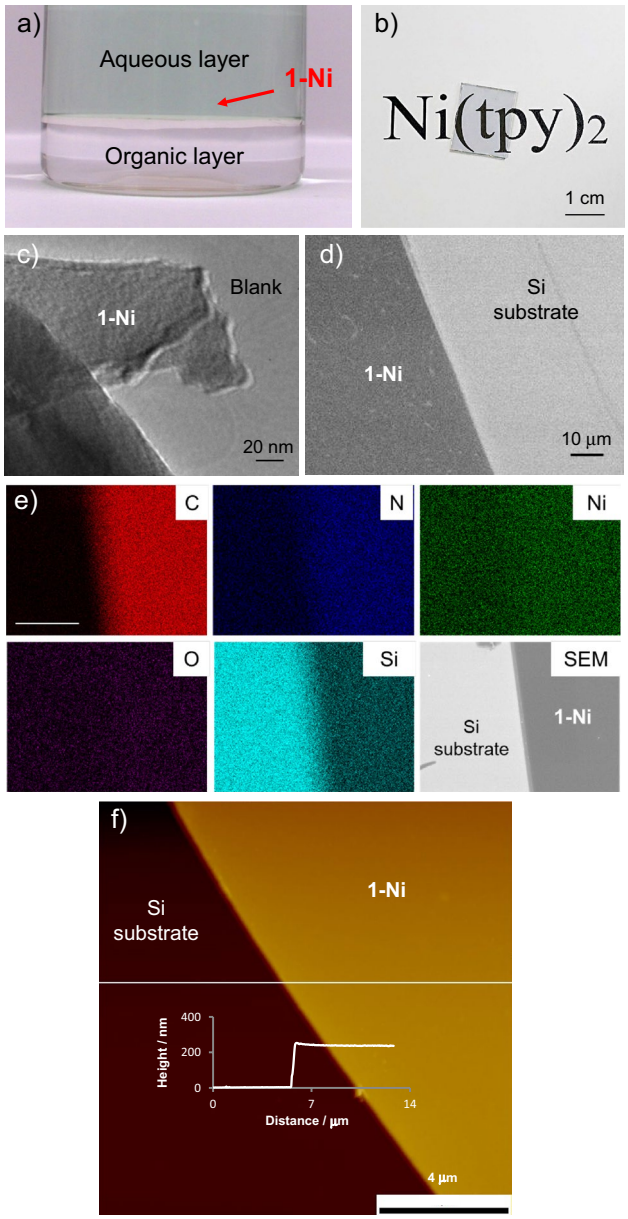

Fig. 2 Synthesis and morphology identification of **1-Ni**. **a** **1-Ni** synthesized by the interfacial coordination reaction. **b** Photograph of transparent **1-Ni** film covering an ITO/glass substrate. **c** TEM image of **1-Ni**. **d** SEM image of **1-Ni**. **e** SEM/EDS mapping for constitution elements of **1-Ni** on an Si substrate (scale bar: 5 µm). **f** Topographic AFM image of **1-Ni** on a flat Si substrate and the cross-sectional analysis inset

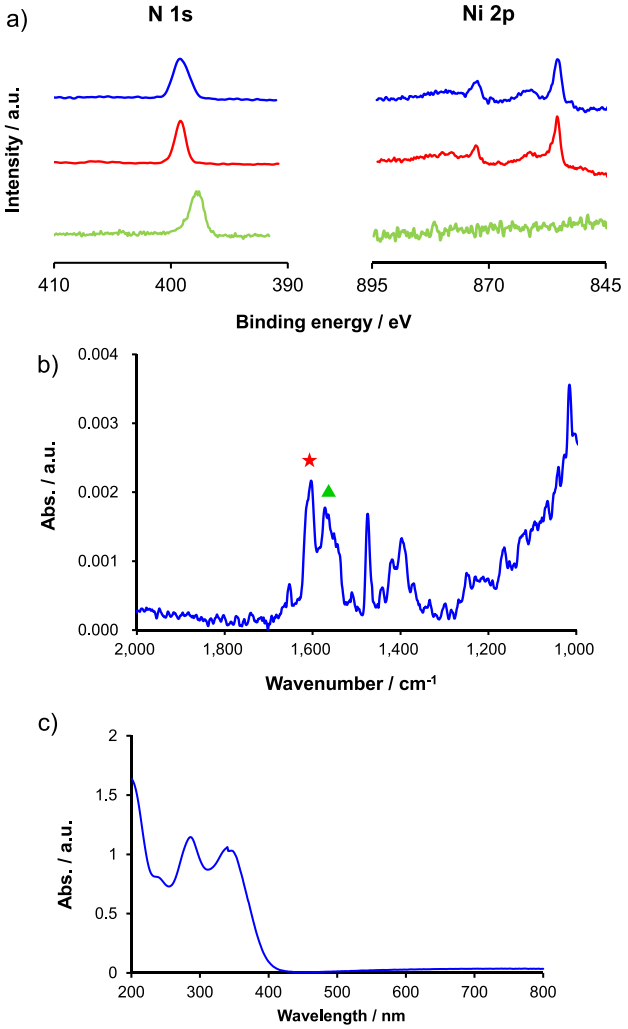

Fig. 3 Spectroscopic characterization of **1-Ni**. **a** XP spectra of **1-Ni** (blue), $[Ni(tpy)_2](BF_4)_2{\cdot}CH_3OH$ (red), and **1** (green) at N 1 s and Ni 2p core levels. **b** ATR-IR spectrum of **1-Ni**. Vibration peaks of C=C stretching and C=O stretching are marked with a red star and a green triangle, respectively. **c** UV–Vis spectrum of **1-Ni** on a quartz substrate (Color figure online)

contains C, N, Ni, and O, exactly the constituent elements of **1-Ni** (Fig. 2e). The atomic force microscopy (AFM) image of **1-Ni** also demonstrates that **1-Ni** is a multi-layered sheet 240 nm thick with a flat surface (Fig. 2f), which was typical for polypyridyl-based CONASHs [32–34]. The thickness is dependent on the concentration of the metal salt used as the aqueous phase at the preparation. While more concentrated $Ni(OAc)_2$ solution (100 mM) gave a thicker CONASH film with ca. 900 nm thickness, diluted solution (5 mM) gave a thinner nanosheet with ca. 15 nm thickness (Fig. S2a–f). These microscopic observations confirm the sheet morphology of **1-Ni**.

We attempted X-ray photoelectron, IR, and UV–Vis spectroscopy techniques to determine the chemical composition and structure of **1-Ni**. In X-ray photoelectron spectra (XPS) (Fig. 3a), the N 1 s peak of **1-Ni** is at 399.2 eV, which underwent a shift to a higher binding energy region from that of the free terpyridine ligand **1** (397.5 eV). This peak shift is attributed to the decrease in electron density around N atoms upon the coordination to Ni^{2+}. This peak shift was also observed in XPS of previously reported bis(terpyridine) iron(II), cobalt(II), and zinc(II) CONASHs [32, 33]. To

compare its spectra, a mononuclear bis(terpyridine)nickel(II) complex, $[Ni(tpy)_2](BF_4)_2$, was synthesized as a reference compound. The N 1 s peak position of **1-Ni** is same as that of $[Ni(tpy)_2](BF_4)_2$ (399.2 eV), definitely proving that terpyridine groups coordinate to Ni^{2+} in **1-Ni**. The peak of non-coordinating nitrogen at 397.5 eV is not apparent in **1-Ni** so that coordination proceeded with little defect less than detection limit of XPS. In addition, Ni $2p_{3/2}$ peak positions are 855.2 eV for **1-Ni** and 855.4 eV for the mononuclear complex, also confirming coordination in **1-Ni**. The quantitative analysis from the peak areas of N 1 s and Ni 2p peaks gives the N: Ni ratio as 6.49: 1. Taking the estimated error of XPS quantitative analysis (10%), the obtained elemental richness exhibits good agreement with that of $[Ni(tpy)_2]^{2+}$ (N: Ni = 6: 1). However, considering the slight excess of nitrogen atom richness, the possibility of structural defects in coordination cannot be eliminated. As explained above, structural defects are one of the major reasons for low crystallinity of our $Ni(tpy)_2$ CONASH film. Given these chemical state and quantitative analyses, XPS defined **1-Ni** as the intended bis(terpyridine)nickel(II) complex nanosheet. In addition, attenuated total reflection infrared (ATR-IR) spectroscopy confirmed formation of a bis(terpyridine)nickel(II) complex nanosheet (Fig. 3b). The C=C stretching mode of **1-Ni** was detected at 1603 cm^{-1}, which shifted by 18 cm^{-1} from 1585 cm^{-1} for the free terpyridine ligand **1**. [32] Considering that the coordination of terpyridine to other metal ions (Fe, Co, and Zn) gave the same trends in peak shifts [32, 33], this is clear evidence of coordination between the terpyridine ligand and nickel ions. Moreover, C=O stretching of acetate ions was observed at 1570 cm^{-1}. According to a previous comprehensive study on IR spectra of acetate ions for various coordination modes [46], the C=O stretching peak of **1-Ni** corresponds to non-coordinating acetate ion. Therefore, acetate ions are included in **1-Ni** as counteranions. UV–Vis spectroscopy also confirmed the formation of $Ni(tpy)_2$ moieties. The UV–Vis spectrum of **1-Ni** deposited on a quartz substrate shows two peaks at 346 nm and 286 nm in the ultraviolet region (Fig. 3c). This is similar to the UV–Vis spectrum of $[Ni(tpy)_2](BF_4)_2$ recorded in CH_3CN (Fig. S3a). Thus, from the spectroscopic analyses described above, we conclude that a bis(terpyridine)nickel(II) diacetate-based CONASH film was synthesized.

3.2 Electrochemistry

Next, electrochemistry of **1-Ni** was investigated. Bis(terpyridine)nickel(II) complex generally exhibits metal-centred redox behaviour based on the $[Ni(tpy)_2]^{3+}/[Ni(tpy)_2]^{2+}$ redox couple and ligand-centred $[Ni(tpy)_2]^{2+}/[Ni(tpy)_2]^{+}$ redox couple [47]. Indeed, $[Ni(tpy)_2](BF_4)_2$ showed a reversible redox peak at $E_{1/2} = 1.14$ V vs. ferrocenium/ferrocene (Fc^+/Fc) in CH_3CN with 0.1 M tetra-*n*-butylammonium hexafluorophosphate (Bu_4NPF_6) as a supporting electrolyte (Fig. S3b). Here we focus on the oxidation behaviour of **1-Ni** because the metal-centred oxidation process is intrinsically unique for **1-Ni**. **1-Ni** prepared with 25 mM $Ni(OAc)_2$ solution (ca. 200 nm in thickness) was used owing to the combination of high capacitance and good transparency (Fig. S2g). To confirm the redox behaviour of **1-Ni**, cyclic voltammetry was conducted in dry CH_2Cl_2 with 1 M Bu_4NPF_6 as a supporting electrolyte (Fig. 4a). The difference of solvent from the mononuclear complex aimed to prevent contamination of water to the solvent. In the cyclic voltammogram obtained under aerobic condition, anodic current around 0.5 V vs. Fc^+/Fc was observed (Fig. S5). The cyclic voltammogram of **1-Ni** showed one chemically reversible oxidation process at $E_{1/2} = 1.22$ V vs. Fc^+/Fc, near the limit of the potential window, consistent with the redox potential of the mononuclear complex (Fig. S3b). The redox activity is totally different from that of the ligand **1**, which did not exhibit a redox behaviour at this potential in 1 M Bu_4NPF_6 in CH_2Cl_2 solution (Fig. S4). Thus, this is attributable to the metal-centred $[Ni(tpy)_2]^{3+}/[Ni(tpy)_2]^{2+}$ redox couple mentioned above. The clearly observable redox peaks suggest that oxidation of $[Ni(tpy)_2]^{2+}$ does not accompany spin reconstruction, while the spin-reconstructing redox couple of $[Co(tpy)_2]^{3+}/[Co(tpy)_2]^{2+}$ in a $Co(tpy)_2$-based CONASH was faintly observable [32]. Thus, the $S = 1$ and 1/2 spin states are suggested for $[Ni(tpy)_2]^{2+}$ and $[Ni(tpy)_2]^{3+}$, respectively, which agrees well with a previous theoretical calculation based on density functional theory [48]. This spin-allowed redox reaction of the $Ni(tpy)_2$ moieties enables fast electron extraction and injection of **1-Ni**. The total charge related to this redox reaction was calculated as 2.3×10^{-5} C from cyclic voltammetry. From the thickness and surface area of **1-Ni**, the charge density stored via the redox reaction of **1-Ni** was calculated as 3.6 C cm^{-3} (3.7×10^{-5} mol cm^{-3}). From the assumption of the hexagonal model structure with $a = b = 4.1$ nm (Fig. S6a), an average interlayer distance was calculated as 0.91 nm. Compared to the estimated interlayer distances of a eclipsed AA stacking structure (1.0 nm) and a staggered AB stacking structure (0.4 nm) (Fig. S6b, c), this is reasonable as a bis(terpyridine)metal(II) CONASH. Chronoamperometry (Fig. 4b) demonstrated that electron transfer through **1-Ni** was completed within 0.5 s. This quick response is similar to that of the $Fe(tpy)_2$ CONASH in our previous study [32]. The potential-step chronoamperogram is highly repeatable over 100 cycles (Fig. 4c). These electrochemical features suggest that **1-Ni** is a good candidate as a redox-active, and transparent material for charge storage.

The change in appearance upon redox reaction was investigated by spectroelectrochemical measurements. UV–Vis spectra of **1-Ni** and oxidized **1-Ni** are shown in Fig. 4d. Upon oxidation of **1-Ni** with an overpotential of + 0.2 V,

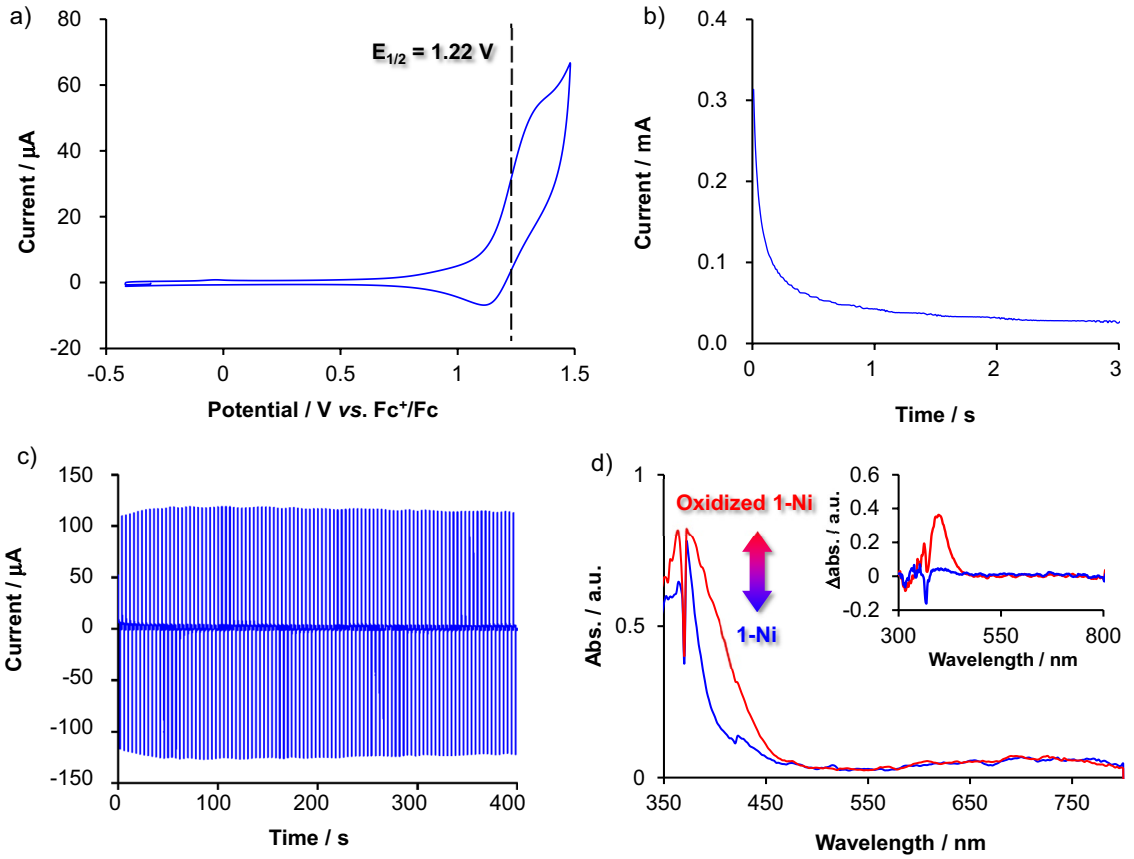

Fig. 4 Electrochemistry of **1-Ni**. **a** Cyclic voltammogram of **1-Ni** in CH_2Cl_2 with 1 M Bu_4NPF_6 (Scan rate: 100 mV s^{-1}). **b** Chronoamperogram of **1-Ni** upon oxidation with an overpotential of + 0.2 V. **c** Repeated chronoamperogram of **1-Ni** for 100 oxidation–reduction cycles with an overpotential of ± 0.2 V. **d** Electrochemical UV–vis spectroscopy of **1-Ni** upon oxidation of **1-Ni**. (inset) Difference spectra between oxidized **1-Ni** and **1-Ni** (red) and between re-reduced **1-Ni** and **1-Ni** on ITO/glass (blue) (Color figure online)

absorption around 400 nm increased, and re-reduction revived the original spectrum. Due to the intense absorption of the ITO electrode, the spectral change below 370 nm was unclear, but there is no spectral change at longer wavelengths. The spectral change was almost limited to the near ultraviolet region (< 450 nm), meaning that the redox reaction of **1-Ni** caused no significant colour change. This is totally different from other electrochromic bis(terpyridine) metal(II)-type CONASHs, in which significant colour change accompanied redox reactions [32, 34, 37]. Thus, **1-Ni** demonstrates unique reversible redox behaviour without any discernible colour change, which makes **1-Ni** attractive to realize future colourless and transparent electronics.

4 Conclusion

We have developed a new redox-active bis(terpyridine) metal(II) complex coordination nanosheet comprising a Ni(II) metal centre. The bis(terpyridine)nickel(II) CONASH was synthesized via a liquid–liquid interfacial coordination reaction at an immiscible water-halocarbon interface, and was successfully characterized with microscopic observations and spectroscopic analyses. The nickel-terpyridine CONASH was redox-active on its $Ni(tpy)_2$ moieties. This redox reaction caused no electrochromism, so that no colour change was visible to eyes. In summary, the bis(terpyridine)nickel coordination nanosheet is a redox-active material possessing flexibility and colourlessness.

Supplementary Information The online version contains supplementary material available at https://doi.org/10.1007/s10904-023-02921-4.

Acknowledgements This study was supported by JSPS KAKENHI (Grant No.: JP19H05460, JP20K15242, JP22K05055, and JP22K14569) and White Rock Foundation. XPS measurements were supported by Advanced Research Infrastructure for Materials and Nanotechnology in Japan (ARIM) of the Ministry of Education, Culture, Sports, Science and Technology (MEXT) Japan (The University of Tokyo, JPMXP1223UT0025). The authors also thank to the Microanalytical Laboratory (The University of Tokyo) for elemental analysis.

Author Contributions KT initiated the research and carried out synthesis, measurements, and analyses. HM supported the synthesis and

electrochemical measurements. HN supervised the research. KT and HN wrote the manuscript and all authors reviewed it.

Funding Open access funding provided by Tokyo University of Science.

Data Availability The all of data supporting the findings of this study are included in the Main text or Supporting information.

Competing interests The authors declare no competing interests.

References

1. K.S. Novoselov, A.K. Geim, S.V. Morozov, D. Jiang, Y. Zhang, S.V. Dubonos, I.V. Grigorieva, A.A. Firsov, Electric field effect in atomically thin carbon films. Science **306**, 666–669 (2004)
2. Q.H. Wang, K. Kalantar-Zadeh, A. Kis, J.N. Coleman, M.S. Strano, Electronics and optoelectronics of two-dimensional transition metal dichalcogenides. Nat. Nanotechnol. **7**, 699–712 (2012)
3. M. Hu, H. Zhang, T. Hu, B. Fan, X. Wang, Z. Li, Emerging 2D MXenes for supercapacitors: status, challenges and prospects. Chem. Soc. Rev. **49**, 6666–6693 (2020)
4. S. Kim, H.C. Choi, Recent advances in covalent organic frameworks for molecule-based two-dimensional materials. ACS Omega **5**, 948–958 (2020)
5. A. Rapakousiou, R. Sakamoto, R. Shiotsuki, R. Matsuoka, U. Nakajima, T. Pal, R. Shimada, M.A. Hossain, H. Masunaga, S. Horike, Y. Kitagawa, S. Sasaki, K. Kato, T. Ozawa, D. Astruc, H. Nishihara, Liquid/liquid interfacial synthesis of 'Click' nanosheet. Chem. Eur. J. **23**, 8443–8449 (2017)
6. Z. Li, M. Smeu, A. Rives, V. Maraval, R. Chauvin, M.A. Ratner, E. Borguet, Towards graphyne molecular electronics. Nat. Commun. **6**, 6321 (2015)
7. R. Matsuoka, R. Sakamoto, K. Hoshiko, S. Sasaki, H. Masunaga, K. Nagoshio, H. Nishihara, Crystalline graphdiyne nanosheets produced at a gas/liquid or liquid/liquid interface. J. Am. Chem. Soc. **139**, 3145–3152 (2017)
8. R. Matsuoka, R. Toyoda, R. Shiotsuki, N. Fukui, K. Wada, H. Maeda, R. Sakamoto, S. Sasaki, H. Masunaga, K. Nagashio, H. Nishihara, Expansion of the graphdiyne family: a triphenylene-cored analogue. ACS Appl. Mater. Interfaces **11**(3), 2730–2733 (2019)
9. M. Zhao, Y. Huang, Y. Peng, Z. Huang, Q. Ma, H. Zhang, Two-dimensional metal–organic framework nanosheets: synthesis and applications. Chem. Soc. Rev. **47**, 6267–6295 (2018)
10. R. Sakamoto, K. Takada, X. Sun, T. Pal, T. Tsukamoto, E.J.H. Phua, A. Rapakousiou, K. Hoshiko, H. Nishihara, The coordination nanosheet (CONASH). Coord. Chem. Rev. **320–321**, 118–128 (2016)
11. R. Sakamoto, K. Takada, T. Pal, H. Maeda, T. Kambe, H. Nishihara, Coordination nanosheets (CONASHs): strategies. Struct. Funct. Chem. Commun. **53**, 5781–5801 (2017)
12. H. Maeda, R. Sakamoto, H. Nishihara, Coordination programming of two-dimensional metal-complex frameworks. Langmuir **32**, 2527–2538 (2016)
13. H. Maeda, K. Takada, N. Fukui, S. Nagashima, H. Nishihara, Conductive coordination nanosheets: sailing to electronics, energy storage, and catalysis. Coord. Chem. Rev. **470**, 214693 (2022)
14. T. Kambe, R. Sakamoto, K. Hoshiko, K. Takada, J.-H. Ryu, S. Sasaki, J. Kim, K. Nakazato, M. Takata, H. Nishihara, π-Conjugated nickel bis(dithiolene) complex nanosheet. J. Am. Chem. Soc. **135**, 2462–2465 (2013)
15. T. Kambe, R. Sakamoto, T. Kusamoto, T. Pal, N. Fukui, T. Shimojima, Z. Wang, T. Hirahara, K. Ishizaka, S. Hasegawa, F. Liu, H. Nishihara, Redox control and high conductivity of nickel bis(dithiolene) complex π-nanosheet. J. Am. Chem. Soc. **136**, 14357–14360 (2014)
16. T. Pal, T. Kambe, T. Kusamoto, M.L. Foo, R. Matsuoka, R. Sakamoto, H. Nishihara, Interfacial synthesis of electrically conducting palladium bis(dithiolene) complex nanosheet. ChemPlusChem **80**, 1255–1258 (2015)
17. T. Pal, S. Doi, H. Maeda, K. Wada, C.M. Tan, N. Fukui, R. Sakamoto, S. Tsuneyuki, S. Sasaki, H. Nishihara, Interfacial transmetallation synthesis of a platinadithiolene nanosheet as a potential 2D topological insulator. Chem. Sci. **10**, 5218–5225 (2019)
18. X. Sun, K.-H. Wu, R. Sakamoto, T. Kusamoto, H. Maeda, X. Ni, W. Jiang, F. Liu, S. Sasaki, H. Masunaga, H. Nishihara, Bis(aminothiolate)nickel nanosheet as a redox switch for conductivity and an electrocatalyst for the hydrogen evolution reaction. Chem. Sci. **8**, 8078–8085 (2017)
19. K. Wada, K. Sakaushi, S. Sasaki, H. Nishihara, Multielectron-transfer-based rechargeable energy storage of two-dimensional cordination frameworks with non-innoscent ligands. Angew. Chem. Int. Ed. **57**, 8886–8890 (2018)
20. J. Park, A.C. Hinckley, Z. Huang, D. Feng, A.A. Yakovenko, M. Lee, S. Chen, X. Zou, Z. Bao, Synthetic routes for a 2D semiconductive copper hexahydroxybenzene metal-organic framework. J. Am. Chem. Soc. **140**, 14533–14537 (2018)
21. X. Huang, P. Sheng, Z. Tu, F. Zhang, J. Wang, H. Geng, Y. Zou, C. Di, Y. Yi, Y. Sun, W. Xu, D. Zhu, A two-dimensional π-d conjugated coordination polymer with extremely high conductivity and ambipolar transport behavior. Nat. Commun. **6**, 7408 (2015)
22. R. Toyoda, N. Fukui, D.H.L. Tjhe, E. Selezneva, H. Maeda, C. Bourgès, C.M. Tan, K. Takada, Y. Sun, I. Jacobs, K. Kamiya, H. Masunaga, T. Mori, S. Sasaki, H. Sirringhaus, H. Nishihara, Heterometallic benzenehexathiolato coordination nanosheets: periodic structure improves crystallinity and electrical conductivity. Adv. Mater. **34**, 2106204 (2022)
23. Y.-C. Wang, C.-H. Chiang, C.-M. Chang, H. Maeda, N. Fukui, I.-T. Wang, C.-Y. Wen, K.-C. Lu, S.-K. Huang, W.-B. Jian, C.-W. Chen, K. Tsukagoshi, H. Nishihara, Two-dimensional bis(dithiolene)iron(II) self-powered UV photodetectors with ultrahigh air stability. Adv. Sci. **8**, 2100564 (2021)
24. R. Makiura, S. Motoyama, Y. Umemura, O. Sakata, H. Kitagawa, Surface nano-architecture of a metal-organic framework. Nat. Mater. **9**, 565–571 (2010)
25. Y. Zhong, B. Cheng, C. Park, A. Ray, S. Brown, F. Mujid, J.-U. Lee, H. Zhou, J. Suh, K.-H. Lee, J.M. Andrew, K. Kang, S.J. Sibener, D.A. Muller, J. Park, Wafer-scale synthesis of monolayer two-dimensional porphyrin polymers for hybrid superlattices. Science **366**, 1379–1384 (2020)
26. R. Sakamoto, K. Hoshiko, Q. Liu, T. Yagi, T. Nagayama, S. Kusaka, M. Tsuchiya, Y. Kitagawa, W.-Y. Wong, H. Nishihara, A photofunctional bottom-up bis(dipyrrinato)zinc(II) complex nanosheet. Nat. Commun. **6**, 6713 (2015)

27. R. Sakamoto, T. Yagi, K. Hoshiko, S. Kusaka, R. Matsuoka, H. Maeda, Z. Liu, Q. Liu, W.-Y. Wong, H. Nishihara, Photofunctionality in porphyrin-hybridized bis(dipyrrinato)zinc(II) complex micro- and nanosheets. Angew. Chem. Int. Ed. **56**, 3526–3530 (2017)
28. W. Dai, L.-T. Lee, A. Schütz, B. Zelenay, Z. Zheng, A. Borgschulte, M. Döbeli, W. Abuillan, O.V. Konovalov, M. Tanaka, A.D. Schlüter, Three-legged 2,2'-bipyridine monomer at the air/water interface: monolayer structure and reactions with Ni(II) Ions from the subphase. Langmuir **33**, 1646–1654 (2017)
29. T. Bauer, Z. Zheng, A. Renn, R. Enning, A. Stemmer, J. Sakamoto, A.D. Schlüter, Synthesis of free-standing. monolayered organometallic sheets at the air/water interface. Angew. Chem. Int. Ed. **50**, 7879–7884 (2011)
30. Z. Zheng, C.S. Ruiz-Vargas, T. Bauer, A. Rossi, P. Payamyar, A. Schütz, A. Stemmer, J. Sakamoto, A.D. Schlüter, Square-micrometer-sized, free-standing organometllic sheets and their square-centimeter-sized multilayers on solid substrates. Macromol. Rapid Commun. **34**, 1670–1680 (2013)
31. Z. Zheng, L. Opilik, F. Schiffmann, W. Liu, G. Bergamini, P. Ceroni, L.-T. Lee, A. Schütz, J. Sakamoto, R. Zenobi, J. VandeVondele, A.D. Schlüter, Synthesis of two-dimensional analogues of copolymers by site-to-site transmetalation of organometallic monolayer sheets. J. Am. Chem. Soc. **136**, 6103–6110 (2014)
32. K. Takada, R. Sakamoto, S.-T. Yi, S. Katagiri, T. Kambe, H. Nishihara, Electrochromic bis(terpyridine)metal complex nanohseets. J. Am. Chem. Soc. **137**, 4681–4689 (2015)
33. T. Tsukamoto, K. Takada, R. Sakamoto, R. Matsuoka, R. Toyoda, H. Maeda, T. Yagi, M. Nishikawa, N. Shinjo, S. Amanno, T. Iokawa, N. Ishibashi, T. Oi, K. Kanayama, R. Kinugawa, Y. Koda, T. Komura, S. Nakajima, R. Fukuyama, N. Fuse, M. Mizui, M. Miyasaki, Y. Yamashita, K. Yamada, W. Zhang, R. Han, W. Liu, T. Tsubomura, H. Nishihara, Coordination nanosheets Based on terpyridine-zinc(II) complexes: as photoactive host materials. J. Am. Chem. Soc. **139**, 5359–5366 (2017)
34. Y. Liu, R. Sakamoto, C.-L. Ho, H. Nishihara, W.-Y. Wong, Electrochromic triphenylamine-based cobalt(II) complex nanosheets. J. Mater. Chem. C **7**, 9159–9166 (2019)
35. R. Arai, M. Li, R. Toyoda, H. Maeda, H. Nishihara, Redox-active, Luminescent coordination nanosheet capsules containing magnetite. Sci. Rep. **10**, 13818 (2020)
36. S. Roy, C. Chakraborty, Interfacial coordination nanosheet based on nonconjugated three-arm terpyridine: a highly color-efficient electrochromic material to converge fast switching with long optical memory. ACS Appl. Mater. & Interfaces **12**, 35181–35192 (2020)
37. J. Komeda, K. Takada, H. Maeda, N. Fukui, T. Tsuji, H. Nishihara, Chemically laminated 2D bis(terpyridine)metal polymer films: formation mechanism at the liquid-liquid interface and redox rectification. Chem. Eur. J. **28**, e202201316 (2022)
38. M.F. Kuehnel, K.L. Orchard, K.E. Dalle, E. Reisner, Selective photocatalytic CO_2 reduction in water through anchoring of a molecular Ni catalyst on CdS nanocrystals. J. Am. Chem. Soc. **139**, 7217–7223 (2017)
39. C. Arana, M. Keshavarz, K.T. Potts, H.D. Abruña, Electrocatalytic reduction of CO_2 and O_2 with electropolymerized films of vinylterpyridine complexes of Fe, Ni and Co. Inorg. Chim. Acta **225**, 285–295 (1994)
40. X. Ding, B. Yu, B. Han, H. Wang, T. Zheng, B. Chen, J. Wang, Z. Yu, T. Sun, X. Fu, D. Qi, J. Jiang, Porphyrin coordination polymer with dual photocatalytic sites for efficient carbon dioxide reduction. ACS Appl. Mater. Interfaces **14**, 8048–8057 (2022)
41. D. Won, J. Bang, S.H. Choi, K.R. Pyun, S. Jeong, Y. Lee, S.H. Ko, Transparent electronics for wearable electronics application. Chem. Rev. **123**, 9982–10078 (2023)
42. K. Kim, Y.-G. Park, B.G. Hyun, M. Choi, J.-U. Park, Recent advances in transparent electronics with stretchable forms. Adv. Mater. **31**, 1804690 (2019)
43. M. Yoonessi, A. Borenstein, M.F. El-kady, C.L. Turner, H. Wang, A.Z. Stieg, L. Pilon, Hybrid transparent PEDOT:PSS molybdenum oxide battery-like supercapacitors. ACS Appl. Energy Mater. **2**, 4629–4639 (2019)
44. M. Cavazzini, S. Quici, C. Scalena, F. Puntoriero, G.L. Ganga, S. Campagna, Synthesis, characterization, absorption spectra, and luminescence properties of multinuclear species made of Ru(II) and Ir(III) chromophores. Inorg. Chem. **48**, 8578–8592 (2009)
45. K. Namiki, A. Sakamoto, M. Murata, S. Kume, H. Nishihara, Reversible photochromism of a ferrocenylazobenzene monolayer controllable by a single green light source. Chem. Commun. **44**, 4650-4652 (2007). https://doi.org/10.1039/b713107k
46. K. Ito, H.J. Bernstein, The vibrational spectra of the formate, acetate, and oxalate ions. Canadian J. Chem. **34**, 170–178 (1957)
47. R. Prasad, D.B. Scaife, Electro-oxidation and electro-reduction of some iron (II), cobalt(II) and nickel(II) polypyridyl complexes in acetonitrile. J. Electroanal. Chem. **84**, 373–386 (1977)
48. M. Wang, J. England, T. Weyhermüller, K. Weighardt, Electronic structures of "Low-Valent" neutral complexes $[NiL_2]^0$ (S = 0; L = bpy, phen, tpy)–an experimental and DFT computational Study. Eur. J. Inorg. Chem. **2015**, 1511–1523 (2015)